Tomita N, Furukawa K, Okamura N, Tashiro M, Une K, Furumoto S, Iwata R, Yanai K, Kudo Y, Arai H	Brain accumulation of amyloid β protein visualized by positoron emission tomography and BF-227 in Alzheimer's disease patients with or without diabetes mellitus	Geriatr Gerontol Int. 13.215-221	13	215-221	2013
Harada R, Okamura N, Furumoto S, Tago T, Maruyama M, Higuchi M, YosikawaT, Arai H, Iwata R, Kudo Y, Yanai K	Comparison of the binding characteri stics of [(18)F]THK- 523 and other amyloid imaging tracers to Alzheimer's disease patholopgy	ur J Nucl Med Mol Imaging 40.125-132	40	125-132	2013
Furumoto S, Okamura N, Furukawa K, Tashiro M, Ishikawa Y, Sugi K, Tomita N, Waragai M, Harada R, Tago T, Iwata R, Yanai K, Arai H, Kudo Y	A (18)F-Labeled BF-227 Derivative as a Potential Radioligand for Imaging Dense Amyloid Plaques by Positron Emission Tomography	Mol Imaging Biol.15.497-506	15	497-506	2013
Shidahara M,Tashiro M,Okamura N,Furumoto S,Furukawa K,Watanuki S,Hiraoka K,Miyake M,Iwata R,Tamura H,Arai H,Kudo Y,Yanai K.	Evaluation of the biodistribution and radiation dosimetry of the 18F-labelled amyloid imaging probe [18F]FACT in humans.	EJNMMI Res.3.32-41	3	32-41	2013
Harada R,Okamura N,Furumoto S,Yoshikawa T, Arai H,Yanai K,Kudo Y.	Use of a Benzimidazole Derivative BF-188 in Fluorescence Multispectral Imaging for Selective Visualization of Tau Protein Fibrils in the Alzheimer's Disease Brain.	Mol Imaging Biol.16.19-27	16	19-27	2013

Maruyama.M, Shimada H, Suhara T, Shinotoh H,Bin J,Maeda J,M.R.Z, Trojanowski.J.Q,Lee V.M.Y, Ono M,Masamoto K,Takano H,Sahara N,Iwata N,Okamura N, Furumoto S, Kudo Y, Chang Q,Saido C.T,Takashima A,Jada L,M.K.J,Aoki I,Ito H,Higuchi M.	Imaging of Tau Pathology in a Ttauopathy Mouse Model and in Alzheimer Patients Compared to Normal Controls.	Neuron 79.1094 - 1108	79	1094-1108	2013
Shidahara M, Tashiro M, Okamura N, Furumoto S, Furukawa K, Watanuki S, Hiraoka K, Miyake M, Iwata R, Tamura H, Arai H, Kudo Y, Yanai K	Evaluation of the biodistribution and radiation dosimetry of the ^{18}F-labelled amyloid imaging probe [^{18}F]FACT in humans	EJNMMI Res	3	32-41	2013
Okamura N,Furumoto S,Harada R,Tago T,Yoshikawa T,Fodero-Tavoletti M,Mulligan R S,Villemagne V L, Akatsu H,Yamamoto T, Arai H, Iwata R,Yanai K., Kudo Y	Novel 18F-labeled arylquinoline derivatives for non-invasive imaging of tau pathology in Alzheimer's disease	Journal of Nuclear Medicine		Accepted	2013
Furumoto S, Okamura N, Furukawa K, Tashiro M, Ishikawa Y, Sugi K, Tomita N, Waragai M, Harada R, Tago T, Iwata R, Yanai K, Arai H, Kudo Y	A (18)F-Labeled BF-227 Derivative as a Potential Radioligand for Imaging Dense Amyloid Plaques by Positron Emission Tomography	Mol Imaging Biol		Accepted	2013
Niu K,Guo H,Guo Y,Ebihara S,Asada M,Ohrui T,Furukawa K,Ichinose M,Yanai K,Kudo Y,Arai H,Okazaki T,Nagatomi R.	Royal jelly prevents the progression of sarcopenia in aged mice in vivo and in vitro	Journal of Gerontology:Biological Sciences		Accepted	2013

Harada R, Okamura N, Furumoto S, Tago T, Maruyama M, Higuchi M, YosikawaT, Arai H, Iwata R, Kudo Y, Yanai K	Comparison of the binding characteri stics of [(18)F]THK-523 and other amyloid imaging tracers to Alzheimer's disease patholopgy	Eur J Nucl Med Mol Imaging	40	125-132	2013
Tomita N, Furukawa K, Okamura N, Tashiro M, Une K, Furumoto S, Iwata R, Yanai K, Kudo Y, Arai H	Brain accumulation of amyloid ß protein visualized by positoron emission tomography and BF-227 in Alzheimer's disease patients with or without diabetes mellitus	Geriatr Gerontol Int	13	215-221	2013
Villemagne V L, Furumoto S, Fodero-Tavoletti M, Harada R, Mulligan R S, Kudo Y, Masters C L, Yanai K, Rowe C C, Okamura N	The challenges of tau imaging	Future Neurology	7	409-421	2012
Furukawa K, Ikeda S, Okamura N, Tashiro M, Tomita N, Furumoto S, Iwata R,Yanai K, Kudo Y, Arai H	Cardiac positron-emission tomography images with an amyloid-specific tracer in familial transthyretin-related systemic amyloidosis	Circulation	125	556-557	2012

研究成果の刊行に関する一覧表

書籍

著者氏名	論文タイトル名	書籍全体の編集者名	書籍名	出版社名	出版地	出版年	ページ
工藤幸司 荒井啓行	脳アミロイドーシス	田村和夫	血液症候群（第2版） 別冊 日本臨床	株式会社日本臨床社	大阪市	2013	648 -652

研究成果の刊行物・別刷

Eur J Nucl Med Mol Imaging (2015) 42:1052–1061
DOI 10.1007/s00259-015-3035-4

ORIGINAL ARTICLE

[^{18}F]THK-5117 PET for assessing neurofibrillary pathology in Alzheimer's disease

Ryuichi Harada[1] · Nobuyuki Okamura[1,2] · Shozo Furumoto[3,4] · Katsutoshi Furukawa[5] · Aiko Ishiki[5] · Naoki Tomita[5] · Kotaro Hiraoka[6] · Shoichi Watanuki[6] · Miho Shidahara[6,7] · Masayasu Miyake[6] · Yoichi Ishikawa[4] · Rin Matsuda[6] · Akie Inami[6] · Takeo Yoshikawa[2] · Tetsuro Tago[4] · Yoshihito Funaki[4] · Ren Iwata[4] · Manabu Tashiro[6] · Kazuhiko Yanai[2] · Hiroyuki Arai[5] · Yukitsuka Kudo[1,4]

Received: 22 December 2014 / Accepted: 3 March 2015 / Published online: 20 March 2015

Abstract
Purpose Visualization of the spatial distribution of neurofibrillary tangles would help in the diagnosis, prevention and treatment of dementia. The purpose of the study was to evaluate the clinical utility of [^{18}F]THK-5117 as a highly selective tau imaging radiotracer.
Methods We initially evaluated in vitro binding of [^{3}H]THK-5117 in post-mortem brain tissues from patients with Alzheimer's disease (AD). In clinical PET studies, [^{18}F]THK-5117 retention in eight patients with AD was compared with that in six healthy elderly controls. Ten subjects underwent an additional [^{11}C]PiB PET scan within 2 weeks.
Results In post-mortem brain samples, THK-5117 bound selectively to neurofibrillary deposits, which differed from the binding target of PiB. In clinical PET studies, [^{18}F]THK-5117 binding in the temporal lobe clearly distinguished patients with AD from healthy elderly subjects. Compared with [^{11}C]PiB, [^{18}F]THK-5117 retention was higher in the medial temporal cortex.
Conclusion These findings suggest that [^{18}F]THK-5117 provides regional information on neurofibrillary pathology in living subjects.

Keywords [^{18}F]THK-5117 · Alzheimer's disease · Tau · Neurofibrillary tangles · PET · Imaging

Electronic supplementary material The online version of this article (doi:10.1007/s00259-015-3035-4) contains supplementary material, which is available to authorized users.

✉ Nobuyuki Okamura
nookamura@med.tohoku.ac.jp

1 Division of Neuro-imaging, Institute of Development, Aging and Cancer, Tohoku University, Sendai 980-8575, Japan

2 Department of Pharmacology, Tohoku University School of Medicine, 2-1, Seiryo-machi, Aoba-ku, Sendai 980-8575, Japan

3 Frontier Research Institute for Interdisciplinary Science, Tohoku University, Sendai 980-8578, Japan

4 Division of Radiopharmaceutical Chemistry, Cyclotron and Radioisotope Center, Tohoku University, Sendai 980-8578, xJapan

5 Department of Geriatrics and Gerontology, Institute of Development, Aging and Cancer, Tohoku University, Sendai 980-8575, Japan

6 Division of Cyclotron Nuclear Medicine, Cyclotron and Radioisotope Center, Tohoku University, Sendai 980-8578, Japan

7 Division of Medical Physics, Tohoku University School of Medicine, Sendai 980-8575, Japan

Introduction

Alzheimer's disease (AD) is the most prevalent form of dementia accounting for more than half of dementia cases. AD is neuropathologically defined by two characteristic protein deposits: senile plaques and neurofibrillary tangles (NFTs) [1]. Senile plaques are composed of extracellular aggregates of amyloid-β peptides (Aβ) [2], while NFTs are composed of twisted filaments termed paired helical filaments of hyperphosphorylated tau protein [3, 4]. Initial tau lesions first appear in the transentorhinal cortex from where they spread to the hippocampus, temporal cortex and other neocortical areas during the course of the disease [1, 5]. As brain tau load is correlated with the severity of cognitive decline and neuronal loss [6–10], tau is considered as a promising therapeutic target for AD [11], and currently, therapeutic trials aimed at modulating tau pathology are underway or being planned [12–14]. For these trials, it is necessary to establish a reliable and non-invasive biomarker that enables the monitoring of tau load in

the living brain [15, 16]. Although tau and phospho-tau levels in the cerebrospinal fluid are useful biomarkers of neurodegeneration in AD [17, 18], they do not provide information on regional tau deposition in the brain. Thus, PET tau imaging would be a promising alternative to noninvasive assessment of tau load in the brain.

In the AD brain, tau aggregates coexist with Aβ plaques in the neocortex. Therefore, selective tau imaging radiotracers are required to assess tau pathology in patients with AD. Recently, several candidates for tau PET tracers have been developed and tested in humans [19–25]. These pilot studies have demonstrated a difference in tracer distribution between patients with AD and healthy elderly subjects. However, the binding selectivity of these tracers for tau pathology has not been fully validated. We have previously screened β-sheet-binding small molecules and have identified a series of compounds that bind NFTs but bind Aβ plaques to a lesser extent [23, 26, 27]. Through a compound optimization process, we developed [^{18}F]THK-5105 and [^{18}F]THK-5117 as putative candidates for tau radiotracer imaging (Fig. 1) [24]. A recent [^{18}F]THK-5105 PET study successfully demonstrated retention of this radiotracer in sites susceptible to tau deposition in the AD brain and its ability to differentiate patients with AD from healthy elderly subjects [28]. However, relatively slower kinetics of [^{18}F]THK-5105 caused high background signal in PET images. On the other hand, [^{18}F]THK-5117 showed faster pharmacokinetics in mice and higher selectivity for tau pathology than [^{18}F]THK-5105 [24], and is thus expected to provided better signal-to-background ratios in PET images. The purpose of this study was to investigate the clinical usefulness of [^{18}F]THK-5117 as a tau-selective PET tracer.

Materials and methods

Autoradiography and in vitro binding assay

Autoradiography and in vitro binding experiments in postmortem brain tissue were conducted using [^{3}H]THK-5117 and [^{3}H]PiB. [^{3}H]PiB (specific activity 2.96 GBq/μmol, radiochemical purity 99 %) was purchased from American Radiolabeled Chemicals (St. Louis, MO). [^{3}H]THK-5117 (specific activity 2.78 GBq/μmol, radiochemical purity 98.2 %) was custom-labelled by Sekisui Medical Inc. (Tokyo, Japan). Experiments were performed under the regulations of the Ethics Committee of Tohoku University School of Medicine. Brain samples were obtained from the Tohoku University Brain Bank. Paraffin-embedded brain sections (8-μm thickness) were used for autoradiography and immunohistochemistry (IHC). For autoradiography, brain sections were incubated with 3 nM of [^{3}H]THK-5117 or [^{3}H]PiB at room temperature for 30 min, and then briefly washed with PBS containing 10 % ethanol. Nonspecific binding was determined in the presence of 3 μM unlabelled THK-5117 or PiB. After drying, the sections were exposed to phosphorimaging plates (BAS-TR2040; GE Healthcare, Little Chalfont, UK) for 2 weeks. The autoradiographic images were obtained using a FLA-7000 phosphorimaging instrument (GE Healthcare) with a spatial resolution of 25×25 μm. Quantitative analysis was performed using ImageQuant TL software (GE Healthcare). For the autoradiographic analysis, images of total binding and nonspecific binding were obtained. Nonspecific binding was determined in the presence of unlabelled compound at 3 μM. The densities in the whole brain sections were measured using ImageQuant software. The amount of specific binding was calculated by subtracting the densities of nonspecific binding from total binding.

Adjacent sections were immunostained using AT8 anti-tau monoclonal antibody (1:20; Innogenetics, Ghent, Belgium), AT100 anti-tau monoclonal antibody (1:40; Pierce Biotechnology, Rockford, IL), or 6F/3D anti-Aβ monoclonal antibody (Dako, Glostrup, Denmark). For IHC analysis, binary images were created using the automated routine of Image J software, and then the percent area of positive signals per section was calculated using Image J software. Pearson correlation coefficients were calculated to evaluate the relationship between specific binding of radiotracers and the percent area of positive signals measured by IHC. For high-resolution autoradiography, radiolabelled sections were dipped into Kodak autoradiography emulsion type NTB (Carestream Health, Inc., Rochester, NY) at 42 °C, air-dried for 1 h at room temperature, and exposed in the dark at 4 °C for 2 weeks in covered slide boxes with silica. Emulsions were developed in Kodak D-19 developer for 4 min, rinsed in water, fixed with Kodak fixer for 5 min, and washed with running water for 30 min. Images were acquired using an Olympus BX51

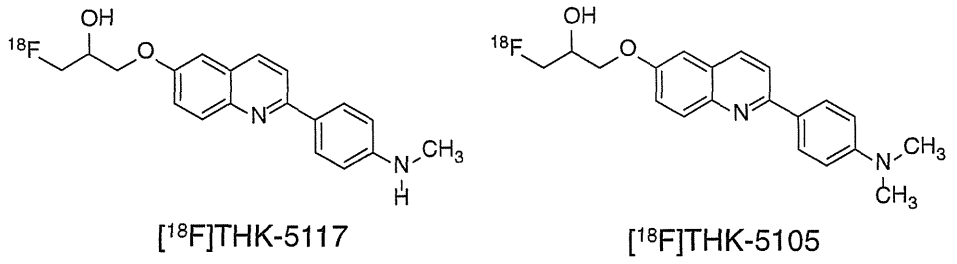

Fig. 1 Chemical structures of [^{18}F]THK-5117 and [^{18}F]THK-5105

microscope (Tokyo, Japan). For β-sheet structure disruption or dephosphorylation of protein in AD brain sections, the sections were treated with 90 % formic acid for 5 min or 16.7 U of *Escherichia coli* alkaline phosphatase (Sigma) at 67 °C for 3 h, respectively [29, 30].

For in vitro binding assays, human brain homogenates (100 μg) from 12 subjects including three healthy controls (HC), eight AD patients and one patient with dementia with Lewy bodies were incubated with 1 nM of [^{3}H]THK-5117 or [^{3}H]PiB. To account for nonspecific binding of the ^{3}H-labelled compound, the above-mentioned reactions were performed in the presence of each unlabelled compound at 1 μM. The binding reactions were incubated for 3 h at room temperature in 200 μL of assay buffer (Dulbecco's PBS, 0.1 % BSA). Separation of bound from free radioactivity was achieved by filtration under reduced pressure (MultiScreen HTS Vacuum Manifold, MultiScreen HTS 96-well 0.65-μm filtration plate; Millipore, Billerica, MA). The filters were washed three times with 200 μL assay buffer, and the filters containing the ^{3}H ligands were incubated in 2 mL of scintillation fluid (Emulsifier-Safe; Perkin Elmer, Boston, MA), and the ^{3}H radioactivity was counted using a beta counter (LS6500 liquid scintillation counter; Beckman Coulter, Brea, CA). Insoluble Aβ and tau levels were determined using ELISA as previously described [24]. Two-tailed Pearson correlation coefficients were calculated to assess the relationship between [^{3}H]THK-5117 binding and [^{3}H]PiB binding and the amount of insoluble protein determined by ELISA.

Radiosynthesis for clinical PET study

[^{18}F]THK-5117 and [^{11}C]PiB were prepared in the Cyclotron and Radioisotope Center, Tohoku University. [^{18}F]THK-5117 was synthesized by nucleophilic substitution of the tosylate precursor, (2-(4-methylaminophenyl)-6-[[2-(tetrahydro-2H-pyran-2-yloxy)-3 -tosyloxy]propoxy]quinoline (THK-5119), as described previously [24]. Details on the radiosynthesis of [^{18}F]THK-5117 will be described elsewhere (Furumoto et al., unpublished data). Injectable solutions of [^{18}F]THK-5117 were prepared with a radiochemical purity of >95 % and a specific activity of 357±270 GBq/μmol. [^{11}C]PiB was synthesized by a loop method using ^{11}C-methyl triflate as described previously [31]. Injectable solutions of [^{11}C]PiB were obtained with a radiochemical purity of >95 % and a specific activity of 240±48 GBq/μmol.

Subjects and patients

A total of 14 subjects including eight patients with AD and six age-matched HCs participated in the [^{18}F]THK-5117 PET study. Among these subjects, five patients and five HCs underwent an additional [^{11}C]PiB PET scan within 2 weeks. Diagnosis of probable AD was based on the criteria of the National Institute of Neurological and Communicative Disorders and Stroke and the Alzheimer's Disease Related Disorders Association (NINCDS-ADRDA). The HCs were recruited from the local area by poster advertisements. These volunteers were taking no centrally acting medications, had no cognitive impairment, and had no cerebrovascular lesions identified on MRI. All HCs underwent the same neuropsychological evaluation as the AD patients. All subjects were screened using a questionnaire and their medical history was examined. Subjects with conditions potentially affecting the central nervous system were excluded. In addition, none of the subjects had asymptomatic cerebral infarction detected on T2-weighted MRI. Clinical PET studies were performed under the regulations of the Ethics Committee of the Tohoku University Hospital. After complete description of the study to the patients and controls, written informed consent was obtained from the subjects or their guardians.

PET and MRI image acquisition

PET imaging was performed using an Eminence STARGATE scanner (Shimadzu, Kyoto, Japan). After intravenous injection of 185 MBq of [^{18}F]THK-5117 or 296 MBq of [^{11}C]PiB, dynamic PET images were obtained for 90 min ([^{18}F]THK-5117) or 70 min ([^{11}C]PiB) with the subject's eyes closed. MR scans were performed in all subjects. T1-weighted and T2-weighted MR images were obtained using a SIGNA 1.5-T machine (General Electric, Milwaukee, WI). With the T1-weighted MR acquisitions, a three-dimensional volumetric acquisition of a T1-weighted gradient echo sequence produced a gapless series of thin axial sections using a vascular TOF SPGR sequence (echo time/repetition time 2.4/50 ms, flip angle 45°, acquisition matrix 256×256, 1 excitation, field of view 22 cm, slice thickness 2.0 mm).

Image analysis

Standardized uptake value (SUV) images of [^{18}F]THK-5117 and [^{11}C]PiB were obtained by normalizing tissue radioactivity concentration by injected dose and body weight. MRI T1 images were coregistered to the early PET images (0 – 10 min after injection) for each subject using statistical parametric mapping software (SPM8; Wellcome Department of Imaging Neuroscience, UCL, London, UK). PET images were processed using a semiautomatic region of interest (ROI) method as previously described [28]. The ratio of regional SUV to cerebellar cortex SUV (SUVR) was used as an index of tracer retention. Coregistered MRI and PET images were spatially normalized to a MRI T1 template in Talairach space using SPM8. After spatial normalization, regional SUVs were sampled using PMOD software. ROIs were placed on individual axial images in the cerebellar hemisphere, ventrolateral prefrontal cortex (Brodmann's areas, BA, 10, 44, 45 and 46),

dorsolateral prefrontal cortex (BA 9), orbitofrontal cortex (BA 11 and 12), superior temporal cortex (BA 22), inferior temporal cortex (BA 20 and 37), parietal cortex (BA 39 and 40), occipital cortex (BA 17, 18 and 19), anterior cingulate cortex, posterior cingulate cortex, hippocampus, parahippocampal gyrus, putamen and subcortical white matter. Average neocortical tau and Aβ burden were expressed as the average SUVR for the following cortical ROIs: the ventrolateral prefrontal, parietal, superior temporal, inferior temporal and posterior cingulate cortices. ROIs and time–activity curves (TACs) were compared between the five patients with AD and five HCs who underwent both [^{18}F]THK-5117 and [^{11}C]PiB PET scans. In addition, MRI-based correction of PET images for partial volume effects was carried out using PMOD (ver. 3.4) software (PMOD Technologies Ltd., Adliswil, Switzerland). Both the spill-out from grey matter and the spill-in from white matter were corrected using the Muller-Gartner method [32].

Statistical analysis

Pearson correlation coefficients were calculated to assess the relationship between ^{3}H-labelled tracer binding and IHC data. The Mann-Whitney *U* test was used for comparison of group differences in clinical variables. Repeated measures analysis of variance (ANOVA) followed by Sidak's multiple comparisons test were used to compare regional SUVR values between HC and AD groups, and to compare regional SUVR values between [^{18}F]THK-5117 and [^{11}C]PiB. Differences in SUVR TACs were also evaluated by repeated measures ANOVA followed by the Bonferroni's multiple comparison test. Correlations between tracer retention and cognitive parameters were examined using a nonparametric Spearman's rank correlation analysis. Effect size coefficients (Cohen's *d*) were calculated for the evaluation of group differences in PET measurements. Statistical significance for each analysis was defined as $P<0.05$. Data are presented as means±standard deviations (SD). Analyses were performed using GraphPad Prism5 software (GraphPad, San Diego, CA).

Results

Characterization of THK-5117 binding to post-mortem brain tissues

On [^{3}H]THK-5117 autoradiograms of AD mesial temporal sections, [^{3}H]THK-5117 revealed a laminar distribution in the deep layer of the grey matter (Fig. 2a), which differed substantially from the dotted pattern of [^{3}H]PiB (Fig. 2b). The distribution of [^{3}H]THK-5117 matched the tau IHC in serial sections (Fig. 2c). In addition, microautoradiography of these sections showed the

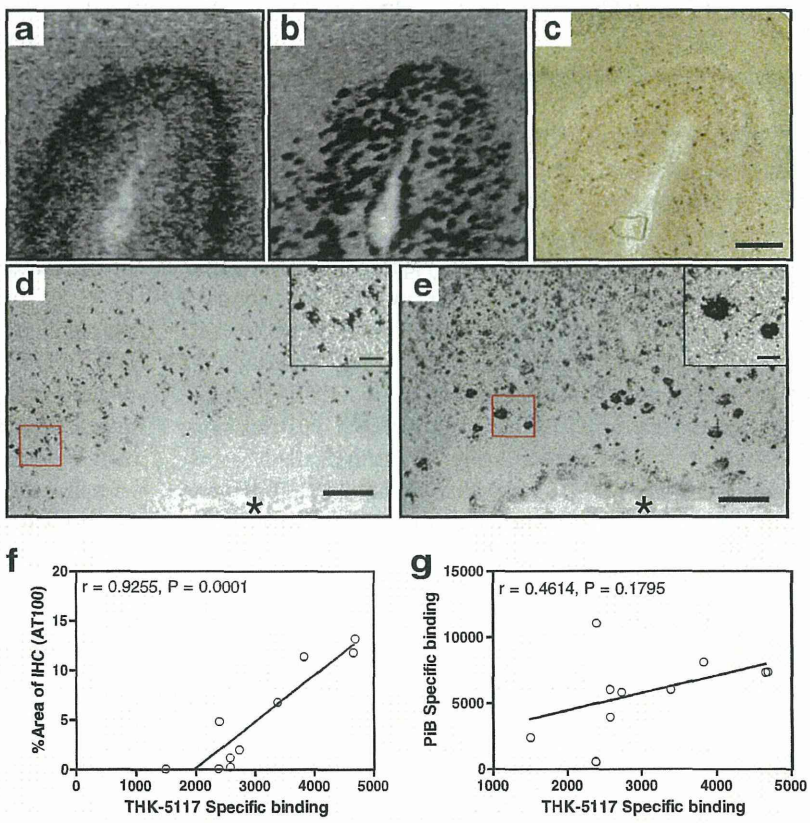

Fig. 2 **a–c** In vitro autoradiography of [^{3}H]THK-5117 (**a**) and [^{3}H]PiB (**b**) in a temporal section from a patient with AD, and immunostaining with anti-tau (**c**, *scale bar* 400 μm). **d**, **e** Microautoradiographic images of [^{3}H]THK-5117 (**d**) and [^{3}H]PiB (**e**) binding in the entorhinal cortex of brain sections from an AD patient. *Inset* Magnified images of neurofibrillary tangles and amyloid plaques labelled with [^{3}H]THK-5117 and [^{3}H]PiB, respectively (*asterisks* same blood vessel, *scale bars* 200 μm). **f**, **g** Correlation analysis of specific [^{3}H]THK-5117 binding and percent area of tau IHC (**f**) and specific [^{3}H]PiB binding (**g**) in brain sections from AD patients

selective binding ability of [^{3}H]THK-5117 to NFTs (Fig. 2d) and [^{3}H]PiB binding to Aβ plaques (Fig. 2e). [^{3}H]THK-5117 did not bind to diffuse Aβ deposits in the striatal sections which were labelled with [^{3}H]PiB (data not shown). Quantitative analysis of the autoradiographic images indicated that the amount of specific binding of [^{3}H]THK-5117 was significantly correlated with the area of positive tau immunostaining (r=0.926, P=0.0001; Fig. 2f), but not with that of Aβ-positive immunostaining (r=0.307, P=0.42) or the amount of [^{3}H]PiB binding (r=0.461, P=0.46; Fig. 2g). The binding selectivity of [^{3}H]THK-5117 to tau was further supported by an in vitro binding assay using human brain homogenates (Supplementary Tables 1 and 2). In AD brain sections, [^{3}H]THK-5117 binding disappeared after the destruction of the β-sheet structure with formic acid, suggesting that the β-sheet structure is necessary for the binding of THK-5117 to tau deposits. However, THK-5117 binding was not influenced by the dephosphorylation of tau deposits, suggesting that the phosphorylation state of tau does not affect THK-5117 binding (Fig. 3a–i). Furthermore, THK-5117 labelled both 3R and 4R isoforms of tau, and both intracellular and extracellular tau in AD brain sections (Fig. 3j–s).

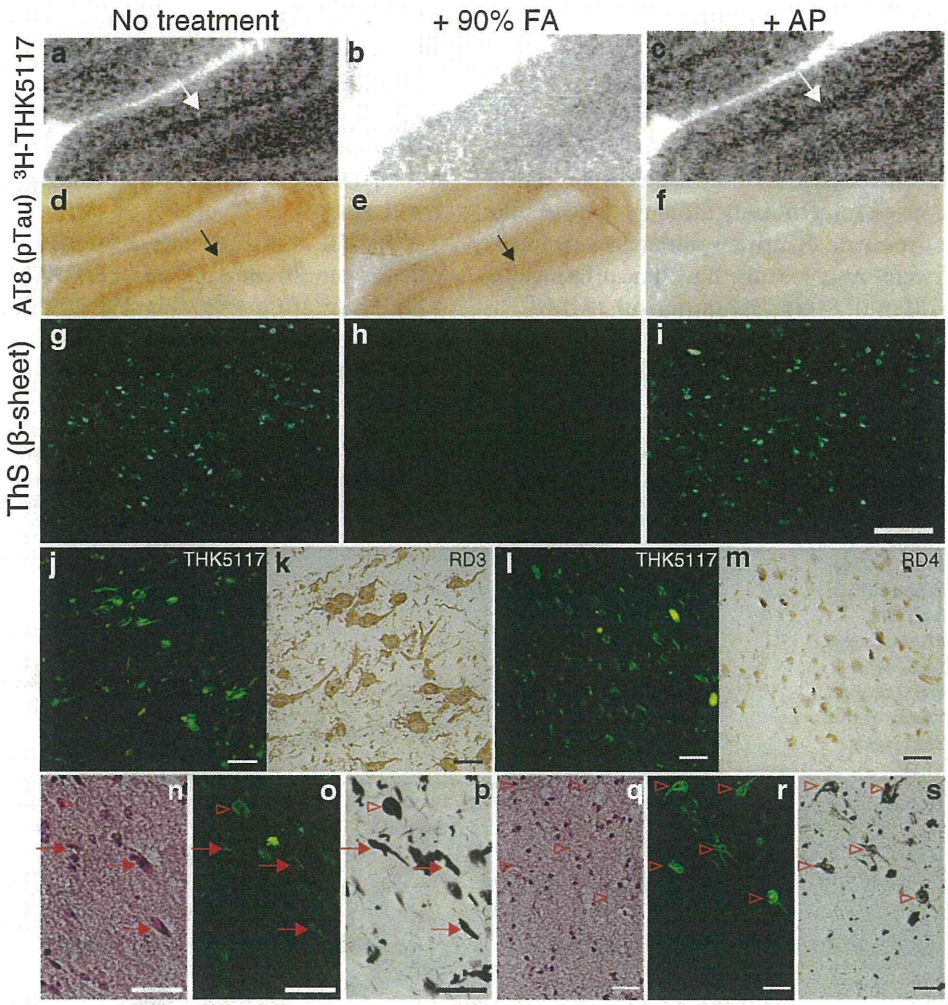

Fig. 3 Analysis of binding targets of THK-5117 in post-mortem AD brain sections. **a** [^{3}H]THK-5117 shows a laminar distribution in the deep layer in the grey matter (*white arrow*) of a brain section from an 82-year-old woman with AD. **b**, **c** Formic acid pretreatment has disrupted the binding of [^{3}H]THK-5117 (**b**), while pretreatment with alkaline phosphatase has failed to disrupt the binding of [^{3}H]THK-5117 (**c**). **d–i** The complete disruption of β-sheet structure and dephosphorylation are confirmed by anti-phosphorylated tau (AT8) IHC (**d–f**) and thioflavin-S fluorescence staining (**g–i**). **j–m** In post-mortem brain sections from a 92-year-old woman with AD immunostained with RD3 (3R tau, **k**) and RD4 (4R tau, **m**) and the same sections stained with THK-5117 (**j**, **l**), both 3R and 4R tau isoforms comprising NFTs are clearly stained with THK-5117. **n–s** In the entorhinal cortex, THK-5117 clearly stains both intracellular NFTs (*red arrows*, **o**), which are basophilic on haematoxylin and eosin (H&E) staining (**n**), and extracellular NFTs (*red arrowheads*, **r**), that is ghost tangles seen as loosely packed pale eosinophilic fibrils on H&E staining (**q**); these staining patterns are consistent with those of Gallyas Braak silver staining (**p**, **s**). *Scale bars* **i** 200 μm, **j–s** 50 μm

Table 1 Demographic characteristics of the healthy controls and patients with Alzheimer's disease

Characteristic	Healthy control (n=6)	Alzheimer's disease (n=8)
Age (years), mean±SD	73.0±5.1	79.8±10.6
Gender (M/F), n	4/2	2/6
Years of education, mean±SD	14.7±2.3	12.1±2.7
Cognitive test scores, mean±SD		
Clinical Dementia Rating	0.0	2.0±0.8
Mini-Mental State Examination	28.7±1.6	18.5±4.6*
Alzheimer's Disease Assessment Scale – cognitive subscale	5.2±2.0	23.8±10.2*
Logical memory II	11.0±5.8	0.9±1.5*

*P<0.05

Clinical PET studies in healthy elderly controls and patients with AD

The demographic characteristics of the subjects are shown in Table 1. Age was not significantly different between the two groups. As expected, significant differences between the two groups were observed for the Clinical Dementia Rating, Mini-Mental State Examination (MMSE), Alzheimer's Disease Assessment Scale – cognitive subscale (ADAS-cog), and logical memory II scores. No toxic events related to the drugs used in this study were observed.

[^{18}F]THK-5117 showed rapid entry into the brain after intravenous administration (Fig. 4). In HCs, TACs for the cerebellum and neocortical regions were nearly identical (Fig. 4a). In patients with AD, the TAC for the inferior temporal cortex, which is known to contain high concentrations of tau protein deposits in AD patients, showed more retention of [^{18}F]THK-5117 at later time-points than the TAC for the cerebellum (Fig. 4b). As shown in Fig. 4c, SUVR TACs for the inferior temporal cortex were significantly different between AD patients and HCs (repeated measures ANOVA, interaction, F= 14.32, df=27, P<0.0001). After Bonferroni correction, SUVR in AD patients was significantly higher from 25 min after injection than in HCs, and reached a plateau at 50 min after injection (Fig. 4c). The TACs of [^{11}C]PiB for the same AD patients as in Fig. 4b are shown in Fig. 4d. [^{11}C]PiB retention in the frontal cortex was relatively higher than that in the inferior temporal cortex, in contrast to higher retention of [^{18}F]THK-5117 in the inferior temporal cortex than in the frontal cortex.

[^{18}F]THK-5117 PET images in a HC (78-year-old man, MMSE score 30) and a patient with AD (72-year-old woman, MMSE score 10) are shown in Fig. 5a. [^{18}F]THK-5117 retention in the inferior temporal and parietal cortices was evident in the patient with AD while it was not in the HC (Fig. 5b).

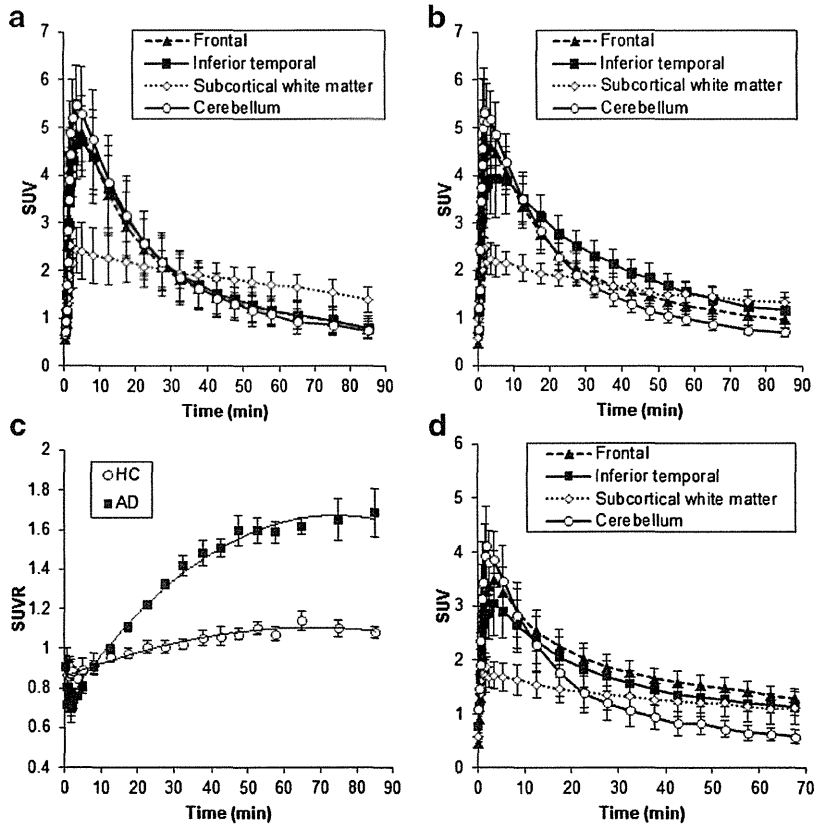

Fig. 4 **a**, **b** [^{18}F]THK-5117 SUV TACs in the cerebellum, inferior temporal cortex and ventrolateral prefrontal cortex of 5 HCs (**a**) and five patients with AD (**b**). **c** [^{18}F]THK-5117 SUVR TACs in the inferior temporal cortex of 5 HCs (*open circles*) and five patients with AD (*filled squares*). **d** [^{11}C]PiB SUV TACs in the cerebellum and inferior temporal cortex and frontal cortex of five patients with AD. Each point represents the mean±SD

Moreover, [^{11}C]PiB retention in the frontal cortex and precuneus was more pronounced than [^{18}F]THK-5117 retention in the same patient (Fig. 5a). Regional tracer uptake was compared between five HC and five patients with AD who underwent both [^{18}F]THK-5117 and [^{11}C]PiB PET scans. [^{18}F]THK-5117 SUVR values for the orbitofrontal, superior and inferior temporal, parietal and posterior cingulate cortices, as well as for the parahippocampal gyrus were significantly greater in patients with AD than in HCs (Table 2). As previously reported, compared to HCs, patients with AD showed significantly greater [^{11}C]PiB retention in the broad neocortical regions, and in patients with AD [^{11}C]PiB SUVR values were greater than [^{18}F]THK-5117 SUVR values in the neocortex except the inferior temporal cortex. In HC subjects, [^{18}F]THK-5117 SUVR was greater than [^{11}C]PiB SUVR in the hippocampus. Both [^{18}F]THK-5117 and [^{11}C]PiB showed higher retention in the subcortical white matter than the other regions in HCs; however, tracer uptake in the subcortical white matter was nearly identical between HCs and patients with AD. In HCs, [^{18}F]THK-5117 additionally showed higher retention than [^{11}C]PiB in the putamen; however, [^{18}F]THK-5117 retention in the putamen was not significantly elevated in patients with AD.

As tau pathology was frequently observed at the site of brain atrophy [33], [^{18}F]THK-5117 signals in patients with severe AD might be underestimated due to brain atrophy. Therefore, partial volume correction was performed for [^{18}F]THK-5117 and [^{11}C]PiB PET images (Fig. 6). High [^{18}F]THK-5117 retention was clearly observed in the medial temporal cortex of patients with severe AD after partial volume correction, in contrast to no remarkable retention of [^{11}C]PiB in the same area. [^{18}F]THK-5117 retention tended to increase as a function of dementia severity. Relatively higher and broader neocortical retention of [^{18}F]THK-5117 was observed in patients with severe AD than in those with mild AD. In patients with AD, [^{18}F]THK-5117 SUVR in the inferior temporal cortex was correlated with MMSE score (r=−0.806, P=0.016) of AD patients (Supplementary Fig. 1) but was not correlated with [^{11}C]PiB SUVR (Supplementary Fig. 2).

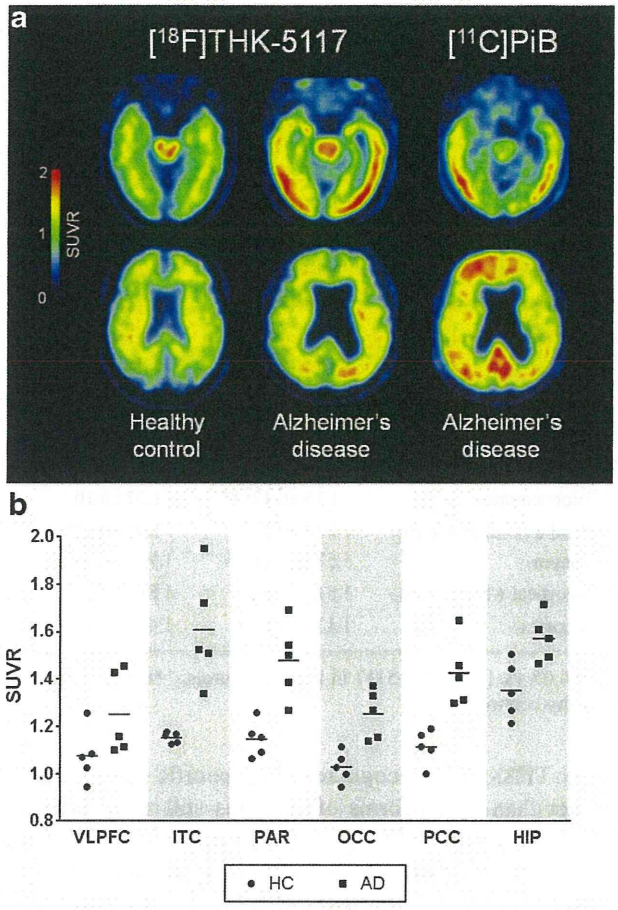

Fig. 5 **a** [^{18}F]THK-5117 PET images from 60 to 80 min after injection in an HC (78 years old, MMSE 30) and in a patient with AD (72 years old, MMSE 10), and [^{11}C]PiB PET images from 40 to 70 min after injection in the same AD patient. **b** [^{18}F]THK-5117 SUVR values in the ventrolateral prefrontal cortex (*VLPFC*), inferior temporal cortex (*ITC*), parietal cortex (*PAR*), occipital cortex (*OCC*), posterior cingulate cortex (*PCC*) and hippocampus (*HIP*) of HCs (*circles*) and patients with AD (*squares*). Horizontal bars indicate mean SUVR values in each group

Discussion

An important property for a tau PET tracer is high binding selectivity to tau over Aβ. In this study, we showed that [^{18}F]THK-5117 binds selectivity to tau by directly comparing [^{18}F]THK-5117 with the Aβ PET tracer PiB. First, the difference in binding targets between [^{18}F]THK-5117 and [^{11}C]PiB was demonstrated in autoradiographic images of AD brain sections, which clearly visualized THK-5117 binding to NFTs and minimal THK-5117 binding to Aβ. Second, the binding assay using human brain tissue demonstrated that THK-5117 binding was significantly correlation with the amount of tau deposits, but not with the amount of Aβ. Third, preferential retention of [^{18}F]THK-5117 was observed in the temporal lobe of patients with AD, which is known as a region of frequent tau deposits. The different neocortical distributions of [^{18}F]THK-5117 and [^{11}C]PiB suggests little [^{18}F]THK-5117 binding to Aβ plaques. Finally, [^{18}F]THK-5117 retention was associated with dementia severity (Fig. 6, Supplementary Fig. 1), consistent with previous results from post-mortem studies [6, 8, 33]. Collectively, this evidence supports the use of [^{18}F]THK-5117 as a selective tau PET tracer. In future work, image-to-autopsy studies are necessary to validate the binding selectivity.

In vitro binding analysis indicated that the β-sheet structure of protein deposits was necessary for THK-5117 binding. However, THK-5117 labelled both 3R and 4R isoforms of tau in AD brain sections, suggesting

Table 2 Regional [^{18}F]THK-5117 and [^{11}C]PiB SUVR values for healthy controls and patients with Alzheimer's disease

Region	[^{18}F]THK-5117			[^{11}C]PiB		
	Healthy control (n=5)	Alzheimer's disease (n=5)	Cohen's d	Healthy control (n=5)	Alzheimer's disease (n=5)	Cohen's d
Ventrolateral prefrontal	1.08±0.11	1.25±0.17	1.18	1.04±0.13	2.31±0.46*/**	3.56
Dorsolateral prefrontal	1.13±0.10	1.20±0.04	0.87	1.14±0.12	2.35±0.47*/**	3.28
Orbitofrontal	0.79±0.09	1.26±0.26*	2.41	0.90±0.17	1.98±0.33*/**	3.97
Superior temporal	1.09±0.09	1.43±0.17*	2.48	1.17±0.13	2.09±0.33*/**	3.39
Inferior temporal	1.15±0.02	1.61±0.23*	2.74	1.10±0.05	2.02±0.47*	2.57
Parietal	1.15±0.08	1.48±0.16*	2.64	1.18±0.10	2.25±0.40*/**	3.41
Occipital	1.03±0.06	1.25±0.10	2.61	1.14±0.09	1.77±0.29*/**	2.70
Anterior cingulate	1.19±0.20	1.36±0.13	0.98	1.19±0.09	2.34±0.42*/**	3.51
Posterior cingulate	1.11±0.07	1.43±0.14*	2.77	1.26±0.13	2.72±0.44*/**	4.25
Hippocampus	1.35±0.12***	1.57±0.10	1.97	1.15±0.09	1.40±0.18	1.62
Parahippocampal gyrus	1.17±0.14	1.43±0.18*	1.69	1.15±0.08	1.72±0.20*	3.53
Putamen	1.57±0.11***	1.77±0.19	1.30	1.26±0.14	2.20±0.41*	2.94
Subcortical white matter	1.81±0.16	1.88±0.20	0.40	1.74±0.18	1.97±0.30	0.90
Neocortex	1.13±0.05	1.42±0.13*	3.05	1.17±0.06	2.29±0.40*/**	3.64

*P<0.05 vs. [^{18}F]THK-5117 in healthy controls, **P<0.05 vs. [^{18}F]THK-5117 in patients with Alzheimer's disease, ***P<0.05 vs. [^{11}C]PiB in healthy controls

that THK-5117 recognizes the specific conformation rather than the isoforms of tau. It is still unclear whether [^{18}F]THK-5117 can detect tau deposits in brains without AD tauopathy in vivo. The binding ability of this tracer to non-AD tau lesions should be examined in the future.

As in the previous [^{18}F]THK-5105 PET study [28], preferential [^{18}F]THK-5117 retention was observed in the temporal lobe of patients with AD. Neurofibrillary pathology in the temporal lobe is more frequent than in the other cortical areas [9, 10] and is observed even in the preclinical AD condition [9, 34]. In addition, tau deposition in the temporal lobe is

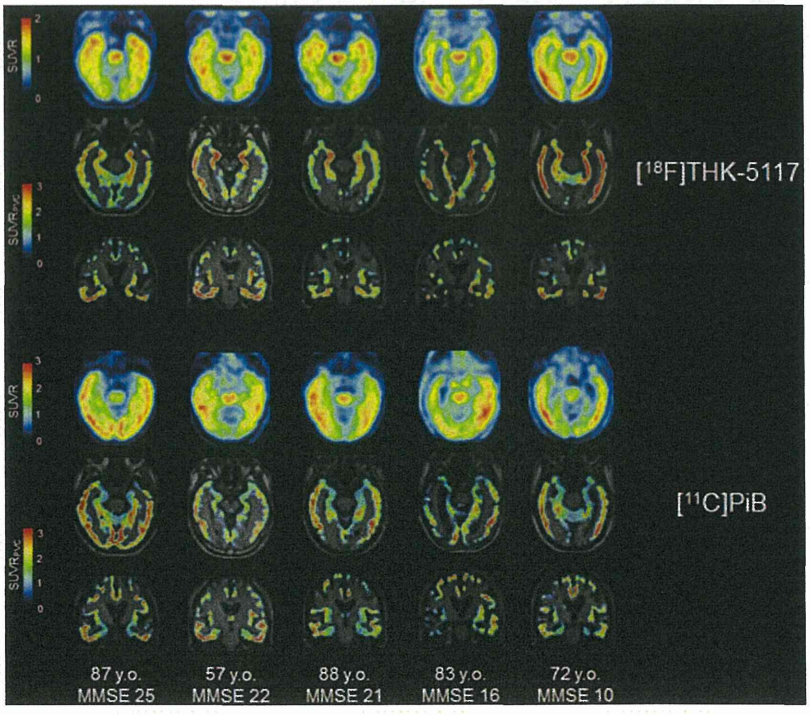

Fig. 6 [^{18}F]THK-5117 and [^{11}C]PiB PET images in five patients with AD after partial volume correction

strongly associated with neurodegeneration and cognitive impairment [7, 33]. As shown in Fig. 6, patients with moderate to severe AD tended to show greater neocortical [^{18}F]THK-5117 retention, which corresponds to Braak stages V/VI. The difference in hippocampal uptake of [^{18}F]THK-5117 between HCs and AD patients was not as robust as we had expected. This may have been caused by the elevated [^{18}F]THK-5117 accumulation in the hippocampus of HCs and the underestimation of hippocampal retention due to atrophy in patients with AD. This result is consistent with the post-mortem finding that hippocampal tau deposits are also frequently observed in nondemented elderly people [35–37].

Many PET tracers have recently been proposed for imaging tau in the human brain. [^{18}F]FDDNP was the first PET tracer that successfully visualized tau pathology in the human brain [38, 39]. However, this tracer reportedly binds nonselectively to both Aβ and tau in AD brains [40]. Recently, [^{11}C]PBB3 has been reported as a selective tau tracer [22]. A PET study successfully demonstrated [^{11}C]PBB3 retention in the hippocampus and neocortex of patients with AD and in the basal ganglia of patients with corticobasal degeneration. However, the short radioactive half-life of ^{11}C restricts the use of [^{11}C]PBB3 to a few PET centres. Two ^{18}F-labelled PET tracers, [^{18}F]T807 and [^{18}F]T808, have recently been reported and clinically tested [19–21]. A first-in-human [^{18}F]T807 PET study has demonstrated that the neocortical [^{18}F]T807 retention follows the known distribution of tau pathology in AD brain [20]. In two patients with AD, [^{18}F]T807 retention was reported to be higher in the lateral temporal cortex than in the frontal cortex. These results are similar to our PET findings. Nevertheless, the main advantage of [^{18}F]THK-5117 over [^{18}F]T807 is its better kinetics in the brain. The time taken to reach the plateau of neocortical SUVR values was shorter for [^{18}F]THK-5117 (50 min after injection) than for [^{18}F]T807 (80 min after injection). However, the use of [^{18}F]T807 may allow more accurate visual interpretation of PET images than the use of [^{18}F]THK-5117 because of the former's negligible white matter retention. [^{18}F]THK-5117 retention in the white matter possibly reflects its binding to β-sheet structures contained in myelin, as observed with other amyloid PET tracers [41]. If sufficient tracer signals are observed in the grey matter of the brain, white matter retention will not lead to the misclassification of scans [42]. However, it is important to develop an optimized PET tracer that shows lower nonspecific binding in the white matter than [^{18}F]THK-5117.

[^{18}F]THK-5117 PET demonstrated high tracer retention in sites susceptible to tau deposition in patients with AD. The in vitro selective binding ability of [^{18}F]THK-5117 to tau was confirmed by directly comparing it with the amyloid PET tracer PiB. Although these results should be considered preliminary due to the small sample size, [^{18}F]THK-5117 is a useful PET tracer for the noninvasive evaluation of tau pathology in patients with AD.

Compliance with Ethical Standards

Funding This study was supported by the research fund from GE Healthcare, the SEI (Sumitomo Electric Industries, Ltd.) Group CSR Foundation, the Industrial Technology Research Grant Program of the NEDO in Japan (09E51025a), Health and Labor Sciences Research Grants from the Ministry of Health, Labor, and Welfare of Japan, a Grant-in-Aid for Scientific Research (B) (23390297), a Grant-in-Aid for Scientific Research on Innovative Areas (26117003) and "Japan Advanced Molecular Imaging Program (J-AMP)" of the Ministry of Education, Culture, Sports, Science and Technology (MEXT), Japan.

Conflicts of interest Yukitsuka Kudo, Nobuyuki Okamura and Shozo Furumoto received research grants from GE Healthcare. Yukitsuka Kudo also received research grants from Sumitomo Electric Industries. Yukitsuka Kudo and Nobuyuki Okamura own stock in Clino Ltd.

Ethical approval All procedures performed in studies involving human participants were in accordance with the ethical standards of the institutional and/or national research committee and with the 1964 Helsinki declaration and its later amendments or comparable ethical standards. This article does not contain any studies with animals performed by any of the authors.

Informed consent Informed consent was obtained from all individual participants included in the study.

References

1. Braak H, Braak E. Neuropathological stageing of Alzheimer-related changes. Acta Neuropathol. 1991;82:239–59.
2. Masters CL, Simms G, Weinman NA, Multhaup G, McDonald BL, Beyreuther K. Amyloid plaque core protein in Alzheimer disease and Down syndrome. Proc Natl Acad Sci U S A. 1985;82:4245–9.
3. Grundke-Iqbal I, Iqbal K, Quinlan M, Tung YC, Zaidi MS, Wisniewski HM. Microtubule-associated protein tau. A component of Alzheimer paired helical filaments. J Biol Chem. 1986;261:6084–9.
4. Grundke-Iqbal I, Iqbal K, Tung YC, Quinlan M, Wisniewski HM, Binder LI. Abnormal phosphorylation of the microtubule-associated protein tau (tau) in Alzheimer cytoskeletal pathology. Proc Natl Acad Sci U S A. 1986;83:4913–7.
5. Braak H, Braak E. Frequency of stages of Alzheimer-related lesions in different age categories. Neurobiol Aging. 1997;18:351–7.
6. Bierer LM, Hof PR, Purohit DP, Carlin L, Schmeidler J, Davis KL, et al. Neocortical neurofibrillary tangles correlate with dementia severity in Alzheimer's disease. Arch Neurol. 1995;52:81–8.
7. Gomez-Isla T, Hollister R, West H, Mui S, Growdon JH, Petersen RC, et al. Neuronal loss correlates with but exceeds neurofibrillary tangles in Alzheimer's disease. Ann Neurol. 1997;41:17–24. doi:10.1002/ana.410410106.
8. Arriagada PV, Growdon JH, Hedley-Whyte ET, Hyman BT. Neurofibrillary tangles but not senile plaques parallel duration and severity of Alzheimer's disease. Neurology. 1992;42:631–9.
9. Wilcock GK, Esiri MM. Plaques, tangles and dementia. A quantitative study. J Neurol Sci. 1982;56:343–56.
10. Arnold SE, Hyman BT, Flory J, Damasio AR, Van Hoesen GW. The topographical and neuroanatomical distribution of neurofibrillary tangles and neuritic plaques in the cerebral cortex of patients with Alzheimer's disease. Cereb Cortex. 1991;1:103–16.

11. Gotz J, Ittner A, Ittner LM. Tau-targeted treatment strategies in Alzheimer's disease. Br J Pharmacol. 2012;165:1246–59. doi:10.1111/j.1476-5381.2011.01713.x.
12. Wischik CM, Harrington CR, Storey JM. Tau-aggregation inhibitor therapy for Alzheimer's disease. Biochem Pharmacol. 2014;88:529–39. doi:10.1016/j.bcp.2013.12.008.
13. Citron M. Alzheimer's disease: strategies for disease modification. Nat Rev Drug Discov. 2010;9:387–98. doi:10.1038/nrd2896.
14. Takashima A. Tau aggregation is a therapeutic target for Alzheimer's disease. Curr Alzheimer Res. 2010;7:665–9.
15. Jack Jr CR, Holtzman DM. Biomarker modeling of Alzheimer's disease. Neuron. 2013;80:1347–58. doi:10.1016/j.neuron.2013.12.003.
16. Cummings JL. Biomarkers in Alzheimer's disease drug development. Alzheimers Dement. 2011;7:e13–44. doi:10.1016/j.jalz.2010.06.004.
17. Arai H, Terajima M, Miura M, Higuchi S, Muramatsu T, Machida N, et al. Tau in cerebrospinal fluid: a potential diagnostic marker in Alzheimer's disease. Ann Neurol. 1995;38:649–52. doi:10.1002/ana.410380414.
18. Itoh N, Arai H, Urakami K, Ishiguro K, Ohno H, Hampel H, et al. Large-scale, multicenter study of cerebrospinal fluid tau protein phosphorylated at serine 199 for the antemortem diagnosis of Alzheimer's disease. Ann Neurol. 2001;50:150–6.
19. Xia CF, Arteaga J, Chen G, Gangadharmath U, Gomez LF, Kasi D, et al. [(18)F]T807, a novel tau positron emission tomography imaging agent for Alzheimer's disease. Alzheimers Dement. 2013;9:666–76. doi:10.1016/j.jalz.2012.11.008.
20. Chien DT, Bahri S, Szardenings AK, Walsh JC, Mu F, Su MY, et al. Early clinical PET imaging results with the novel PHF-tau radioligand [F-18]-T807. J Alzheimers Dis. 2013;34:457–68. doi:10.3233/JAD-122059.
21. Chien DT, Szardenings AK, Bahri S, Walsh JC, Mu FR, Xia CF, et al. Early clinical PET imaging results with the novel PHF-Tau radioligand [F18]-T808. J Alzheimers Dis. 2014;38:171–84. doi:10.3233/Jad-130098.
22. Maruyama M, Shimada H, Suhara T, Shinotoh H, Ji B, Maeda J, et al. Imaging of tau pathology in a tauopathy mouse model and in Alzheimer patients compared to normal controls. Neuron. 2013;79:1094–108. doi:10.1016/j.neuron.2013.07.037.
23. Fodero-Tavoletti MT, Okamura N, Furumoto S, Mulligan RS, Connor AR, McLean CA, et al. 18F-THK523: a novel in vivo tau imaging ligand for Alzheimer's disease. Brain. 2011;134:1089–100. doi:10.1093/brain/awr038.
24. Okamura N, Furumoto S, Harada R, Tago T, Yoshikawa T, Fodero-Tavoletti M, et al. Novel 18F-labeled arylquinoline derivatives for noninvasive imaging of tau pathology in Alzheimer disease. J Nucl Med. 2013;54:1420–7. doi:10.2967/jnumed.112.117341.
25. Villemagne VL, Furumoto S, Fodero-Tavoletti MT, Mulligan RS, Hodges J, Harada R, et al. In vivo evaluation of a novel tau imaging tracer for Alzheimer's disease. Eur J Nucl Med Mol Imaging. 2014;41:816–26. doi:10.1007/s00259-013-2681-7.
26. Okamura N, Suemoto T, Furumoto S, Suzuki M, Shimadzu H, Akatsu H, et al. Quinoline and benzimidazole derivatives: candidate probes for in vivo imaging of tau pathology in Alzheimer's disease. J Neurosci. 2005;25:10857–62. doi:10.1523/JNEUROSCI.1738-05.2005.
27. Harada R, Okamura N, Furumoto S, Tago T, Maruyama M, Higuchi M, et al. Comparison of the binding characteristics of [18F]THK-523 and other amyloid imaging tracers to Alzheimer's disease pathology. Eur J Nucl Med Mol Imaging. 2013;40:125–32.
28. Okamura N, Furumoto S, Fodero-Tavoletti MT, Mulligan R, Harada R, Yates P, et al. Non-invasive assessment of Alzheimer's disease neurofibrillary pathology using 18F-THK5105 PET. Brain. 2014;137:1762–71.
29. Kitamoto T, Ogomori K, Tateishi J, Prusiner SB. Formic acid pretreatment enhances immunostaining of cerebral and systemic amyloids. Lab Invest. 1987;57:230–6.
30. Murayama H, Shin RW, Higuchi J, Shibuya S, Muramoto T, Kitamoto T. Interaction of aluminum with PHFtau in Alzheimer's disease neurofibrillary degeneration evidenced by desferrioxamine-assisted chelating autoclave method. Am J Pathol. 1999;155:877–85.
31. Verdurand M, Bort G, Tadino V, Bonnefoi F, Le Bars D, Zimmer L. Automated radiosynthesis of the Pittsburg compound-B using a commercial synthesizer. Nucl Med Commun. 2008;29:920–6. doi:10.1097/MNM.0b013e328304e0e1.
32. Muller-Gartner HW, Links JM, Prince JL, Bryan RN, McVeigh E, Leal JP, et al. Measurement of radiotracer concentration in brain gray matter using positron emission tomography: MRI-based correction for partial volume effects. J Cereb Blood Flow Metab. 1992;12:571–83. doi:10.1038/jcbfm.1992.81.
33. Whitwell JL, Josephs KA, Murray ME, Kantarci K, Przybelski SA, Weigand SD, et al. MRI correlates of neurofibrillary tangle pathology at autopsy: a voxel-based morphometry study. Neurology. 2008;71:743–9. doi:10.1212/01.wnl.0000324924.91351.7d.
34. Hof PR, Bierer LM, Perl DP, Delacourte A, Buee L, Bouras C, et al. Evidence for early vulnerability of the medial and inferior aspects of the temporal lobe in an 82-year-old patient with preclinical signs of dementia. Regional and laminar distribution of neurofibrillary tangles and senile plaques. Arch Neurol. 1992;49:946–53.
35. Kuzuhara S, Ihara Y, Toyokura Y, Shimada H. A semiquantitative study on Alzheimer neurofibrillary tangles demonstrated immunohistochemically with anti-tau antibodies, in the brains of non-demented and demented old people. No To Shinkei. 1989;41:465–70.
36. Price JL, Morris JC. Tangles and plaques in nondemented aging and "preclinical" Alzheimer's disease. Ann Neurol. 1999;45:358–68.
37. Morris JC, Price JL. Pathologic correlates of nondemented aging, mild cognitive impairment, and early-stage Alzheimer's disease. J Mol Neurosci. 2001;17:101–18.
38. Shoghi-Jadid K, Small GW, Agdeppa ED, Kepe V, Ercoli LM, Siddarth P, et al. Localization of neurofibrillary tangles and beta-amyloid plaques in the brains of living patients with Alzheimer disease. Am J Geriatr Psychiatry. 2002;10:24–35.
39. Small GW, Kepe V, Ercoli LM, Siddarth P, Bookheimer SY, Miller KJ, et al. PET of brain amyloid and tau in mild cognitive impairment. N Engl J Med. 2006;355:2652–63. doi:10.1056/NEJMoa054625.
40. Agdeppa ED, Kepe V, Liu J, Flores-Torres S, Satyamurthy N, Petric A, et al. Binding characteristics of radiofluorinated 6-dialkylamino-2-naphthylethylidene derivatives as positron emission tomography imaging probes for beta-amyloid plaques in Alzheimer's disease. J Neurosci. 2001;21:RC189.
41. Herholz K, Ebmeier K. Clinical amyloid imaging in Alzheimer's disease. Lancet Neurol. 2011;10:667–70. doi:10.1016/S1474-4422(11)70123-5.
42. Vandenberghe R, Van Laere K, Ivanoiu A, Salmon E, Bastin C, Triau E, et al. 18F-flutemetamol amyloid imaging in Alzheimer disease and mild cognitive impairment: a phase 2 trial. Ann Neurol. 2010;68:319–29. doi:10.1002/ana.22068.

Cortical Laminar Binding of PET Amyloid and Tau Tracers in Alzheimer Disease

Yi Li*[1,2], Wai Tsui[1], Henry Rusinek[1], Tracy Butler[1,3], Lisa Mosconi[1], Elizabeth Pirraglia[1], David Mozley[3], Shankar Vallabhajosula[3], Ryuichi Harada[4], Shozo Furumoto[5], Katsutoshi Furukawa[4], Hiroyuki Arai[4], Yukitsuka Kudo[4], Nobuyuki Okamura[4,6], and Mony J. de Leon*[1,7]

[1]Center for Brain Health, New York University, New York, New York; [2]Shandong University, Shandong, China; [3]Cornell University, Ithaca, New York; [4]Institute of Development, Aging, and Cancer, Sendai, Japan; [5]Cyclotron and Radioisotope Center, Sendai, Japan; [6]Tohoku University School of Medicine, Sendai, Japan; and [7]The Steven and Alexandra Cohen Veterans Center at NYU, New York, New York

Neurofibrillary tau pathology and amyloid β (Aβ) plaques, characteristic lesions of Alzheimer disease (AD), show different neocortical laminar distributions. Neurofibrillary-tangle tau pathology tends to be closer to the gray matter–white matter boundary, whereas Aβ is dispersed throughout the width of the cortical ribbon. **Methods:** Using PET radiotracers for tau and Aβ lesions, we developed an image analysis tool to measure the distance of tracer-positive voxels from the gray matter–white matter boundary. We studied 5 AD and 5 healthy subjects with both ^{18}F-THK5117 (tau) and ^{11}C-Pittsburgh compound B (Aβ) PET. **Results:** On average, tau-positive voxels were closer to the white matter than were Aβ-positive voxels. This effect was found for all AD subjects and for all regions, both before and after regionally adjusting for the nonspecific white matter binding of both tracers. The differential laminar pattern was validated through postmortem examination. **Conclusion:** Within cortical lamina, distance measures may be of value in testing PET tracers for their anatomic selectivity.

Key Words: tau; amyloid beta; neocortical binding; PET

J Nucl Med 2015; 56:270–273
DOI: 10.2967/jnumed.114.149229

Senile amyloid plaques and neurofibrillary tangles (tau pathology) are the two characteristic lesions required for a neuropathologic diagnosis of Alzheimer disease (AD) (*1*). On histopathology, amyloid β (Aβ) plaques are extracellular and dispersed throughout the neocortical ribbon (*2*). During the progression of AD, tau tangles initially appear in the hippocampal formation and subsequently in the neocortex (*3*), where they are intracellular and preferentially located in neocortical layers V and VI, closer to the gray matter–white matter boundary (*4*). Analogs of thioflavin T such as ^{11}C-Pittsburgh compound B (PiB) adapted for PET have been validated for imaging Aβ deposits (*5*). Recently, PET compounds have been developed to label tau pathology (*6–8*).

Typically, PET images are analyzed by assessing regional signal uptake in the cerebral cortex, but the distribution of signal within the cortical ribbon is ignored. The objective of this study was to investigate whether the differential spatial distributions of these two lesions in the cortical ribbon of AD patients can be detected with PET imaging. We tested the hypothesis that the bound tau tracer is closer to the gray matter–white matter boundary than is Aβ.

MATERIALS AND METHODS

Participants

Ten subjects were studied: 5 with probable AD (3 women and 2 men; mean age ± SD, 77.4 ± 13.0 y; range, 57–88 y; Mini-Mental State Examination score, 18.8 ± 5.9; Clinical Dementia Rating, 2.0 ± 1.0; education, 12.2 ± 3.6 y) and 5 healthy elderly controls (4 men and 1 woman; mean age, 71.6 ± 4.2 y; range, 67–78 y; Mini-Mental State Examination score, 28.8 ± 1.8; Clinical Dementia Rating, 0; education, 13.6 ± 2.2 y). Written informed consent was obtained from all participants. One AD postmortem autoradiography validation study was conducted using ^{3}H-THK5117 and ^{3}H-PiB. The protocol was approved by the Ethics Committee of Tohoku University Hospital. Controls were recruited by advertisements in the community. AD patients were recruited from the memory clinic of Tohoku University Hospital. The clinical and neuropsychological performance of the participants was assessed by a neurologist and a neuropsychologist in consensus, who were not aware of the PET results. AD was diagnosed according to the criteria of the National Institute of Neurologic and Communicative Disorders and Stroke/Alzheimer's Disease and Related Disorders Association.

Image Acquisition

MR imaging was performed on a SIGNA 1.5-T magnet (GE Healthcare). A 3-dimensional volumetric acquisition of a T1-weighted spoiled gradient recalled sequence produced gapless axial sections (echo time/repetition time, 2.4/50 ms; flip angle, 45°; acquisition matrix, 256 × 256; 1 excitation; field of view, 22 cm; slice thickness, 2.0 mm). The two radiotracers, 6-[(3-^{18}F-fluoro-2-hydroxy)propoxy]-2-(4-methylaminophenyl)quinoline (^{18}F-THK5117) and ^{11}C-PiB, were prepared at the Cyclotron and Radioisotope Center of Tohoku University. ^{18}F-THK5117 was synthesized as described previously (*9*). ^{11}C-PiB PET was synthesized using the 1-step ^{11}C-methyl triflate approach (*10*). PET data were acquired using an Eminence STARGATE PET scanner (Shimadzu) from 0 to 90 min for ^{18}F-THK5117 with a dosage of 185 mBq and from 0 to 70 min for ^{11}C-PiB with dosage of 296 mBq.

Received Sep. 30, 2014; revision accepted Dec. 11, 2014.
For correspondence or reprints contact: Mony J. de Leon, NYU School of Medicine, Department of Psychiatry,145 E. 32 St., 5th Floor, New York, NY 10016.
E-mail: mony.deleon@nyumc.org.
*Contributed equally to this work.
Published online Jan. 15, 2015.

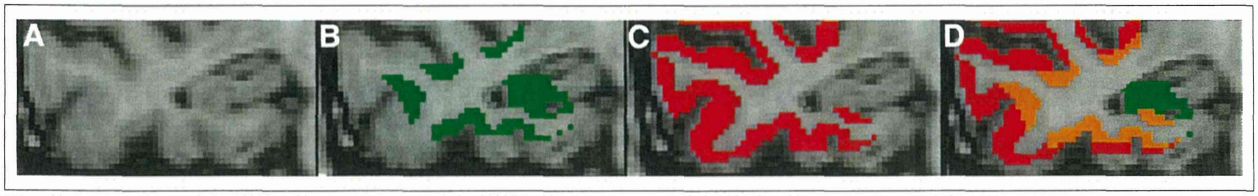

FIGURE 1. (A) T1-weighted MR image of right temporal cortex of AD patient. (B) Tau-positive voxels (green). (C) Amyloid-positive voxels (red). (D) Overlapping tau and amyloid voxels (orange). All are at 1.5-SD cutoff.

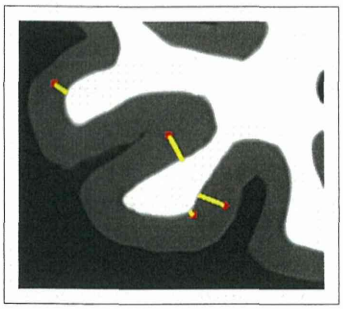

FIGURE 2. Schematic representation of distance[v] image. For each PET tracer, positive gray ribbon voxels (red dots) were defined by statistical threshold and shortest distance to white matter boundary computed (yellow line). Gray matter ribbon and gray matter–white matter boundary are defined by MR imaging.

Image Analysis

For each subject, dynamic PET frames of both ^{18}F-THK5117 and ^{11}C-PiB were realigned using SPM8 software (www.fil.ion.ucl.ac.uk/spm). Standardized uptake value (SUV) images were generated from ^{18}F-THK5117 using the 50- to 80-min frames and from ^{11}C-PiB using the 50- to 70-min frames. All SUV images were coregistered to the corresponding MR imaging volumes using SPM8. MR imaging–determined regions of interest were used to sample the PET images. MR imaging–based regions of interest were determined by Free-Surfer (version 5.1, http://surfer.nmr.mgh.harvard.edu) for the gray and white matter for the entire neocortex (principal outcome) and separately for the frontal, parietal, occipital, and temporal lobes and for the cerebellum. For each tracer, the cerebellar gray matter was used to create regional SUV ratios (SUVRs).

Cutoff cortex values for positive and negative ^{18}F-THK5117 and ^{11}C-PiB PET voxels were regionally defined referencing the mean control SUVR and SD. Cutoffs were tested at 1.5 (Fig. 1) and 1.0 times the SD. A distance[v] measure was generated for all positive cortical voxels for each tracer based on the shortest distance to the MR imaging–defined gray matter–white matter boundary (Fig. 2). To test whether distance[v] distinguished ^{18}F-THK5117 binding from ^{11}C-PiB binding, the distributions in AD subjects were estimated for each of the regions of interest. Voxels located in the neocortex with an apparent thickness of less than 1.0 mm (likely caused by segmentation errors, <10% of total) were excluded from the analysis.

Statistical Analysis

We tested the hypothesis that distance[v] is shorter for tau than for Aβ by the paired *t* test and the nonparametric Wilcoxon signed-rank test. A residual approach was taken to adjust for the confounding effects of nonspecific white matter uptake of the two tracers. Specifically, in the control group, regional regression equations defining the relationships between distance[v] and adjacent white matter uptake were estimated. Subsequently, these regression models were applied to the AD group and used to calculate the AD residuals (residual = actual value minus predicted value). The residuals and actual values were tested. Analyses were performed with SPSS, version 19 (IBM). Results were declared statistically significant when *P* was less than 0.05.

RESULTS

Compared with controls (C), the total neocortex SUVR was higher in AD for both ^{11}C-PiB ($\bar{x}_{SUVR\text{-}C}$ = 1.13 ± 0.04, $\bar{x}_{SUVR\text{-}AD}$ = 1.69 ± 0.17) and ^{18}F-THK5117 ($\bar{x}_{SUVR\text{-}C}$ = 1.12 ± 0.06, $\bar{x}_{SUVR\text{-}AD}$ = 1.31 ± 0.07). The average cortical thickness was 1.90 mm in AD patients and 2.85 mm in controls. For both the 1.5- and the 1.0-SD cutoffs, in all regions the mean distance[v] was significantly shorter for tau than for Aβ. Adjustment for partial-volume artifacts did not change the results (Table 1). All significant test results were confirmed using the Wilcoxon signed-rank test. Figure 1 shows the AD spatial distribution of tau and Aβ tracer binding in the temporal lobe of a representative patient. The individual distance[v] data are in the supplemental data (available online at http://jnm.snmjournals.org).

TABLE 1
Mean Distance[v] and Total Counts for ^{18}F-THK5117– and ^{11}C-PiB–Positive Voxels (1.5-SD Cutoff)

Region	^{18}F-THK5117 (mm)	^{11}C-PiB (mm)	Unadjusted *P*	Regression-adjusted *P*	Number of positive voxels (×10^5)	
					^{18}F-THK	^{11}C-PiB
Total cortex	1.49 ± 0.11	1.73 ± 0.10	0.01	0.02	2.2	11.1
Frontal cortex	1.42 ± 0.06	1.78 ± 0.15	0.01	0.04	0.6	4.3
Parietal cortex	1.32 ± 0.05	1.50 ± 0.05	0.01	0.04	0.4	2.5
Temporal cortex	1.70 ± 0.23	1.89 ± 0.19	0.01	0.01	0.7	2.1
Occipital cortex	1.44 ± 0.13	1.66 ± 0.06	0.01	0.01	0.2	1.0

Data are mean ± SD.

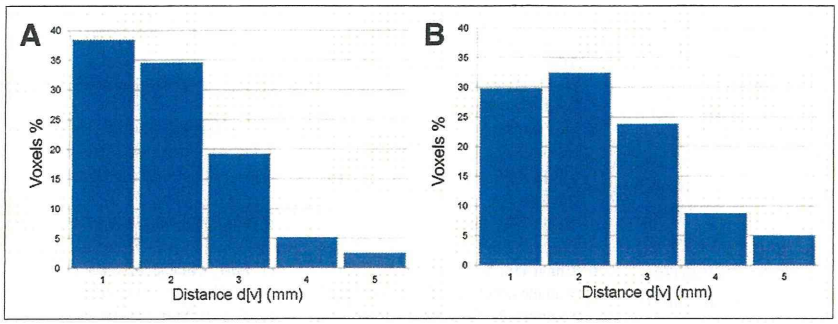

FIGURE 3. AD distance[v] histogram for neocortical ^{18}F-THK5117– and ^{11}C-PiB–positive voxels (1.5 SDs). (A) Distance[v] histogram of ^{18}F-THK5117–positive voxels in total neocortex. (B) Distance[v] histogram of ^{11}C-PiB–positive voxels in total neocortex.

For ^{11}C-PiB at the 1.5-SD cutoff, the total number of positive voxels (1.1×10^6) was approximately 5 times greater than that for ^{18}F-THK5117 (0.2×10^6). Histogram analysis of the neocortical distribution pattern of ^{11}C-PiB– and ^{18}F-THK5117–positive voxels showed that ^{18}F-THK5117 skewed toward shorter distances (Fig. 3). This distribution pattern was not observed in controls (Supplemental Fig. 1).

The postmortem autoradiography study also showed that tau binding localized to the deeper cortical layers, whereas ^{11}C-PiB binding was more widely distributed (Fig. 4).

DISCUSSION

Previous studies have shown a diagnostic value for PiB (*5*) and for THK5117 (*8*) in AD. However, the intralaminar distributions of THK5117 and PiB have not been previously described. In agreement with neuropathologic evidence that tau and Aβ, the principal lesions of AD, have different cortical laminar distributions (*4*), we present the first (to our knowledge) PET imaging confirmation of this distribution pattern. Neurofibrillary pathology in AD is typically found in the deeper cortical lamina whereas plaques are widely distributed (2,4). In agreement, we found with PET that the average distance[v] of tau-positive cortical voxels to the gray matter–white matter boundary is shorter than that of Aβ-positive voxels. We observed this effect in each AD subject and for all regions tested. These PET findings are further supported by our postmortem study using THK5117 and PiB to map Aβ and tau pathology.

Although the distance[v] difference between the imaged tau and Aβ deposits was approximately 0.2 mm, well below the spatial resolution of PET (*11*), because of the large number ($\sim 10^6$) of voxels the effect was significant and observed in all 5 AD patients and in all brain regions. When measured with the Cohen κ (the mean difference between the ^{11}C-PiB and ^{18}F-THK5117 distances, divided by overall SD), the effect was nearly 200%.

Our finding of a 5-fold increased magnitude of Aβ over tau-positive voxels indicates the greater extent of Aβ pathology. These findings are also consistent with neuropathologic findings (*12*) and further contribute to the face validity of PET imaging in AD.

Cross-contamination between adjacent cortical and white matter voxels, each with distinct tracer uptake, is referred to as the partial-volume artifact. To investigate whether our findings can be attributed to this artifact, we generated a conservative control-group–based model that regresses the lesion distance measure on the white matter SUVR. After applying the adjustment to the AD group, the tracer pattern remained significant for all brain regions at the conservative 1.5-SD lesion cutoff.

The current method is of potential interest for subjects experiencing traumatic brain injury, for whom the laminar distribution of the tau pathology is reported to be more superficial (*13*). Future studies will also examine continuous measures of tracer retention, with distance being weighted by the uptake in each voxel.

CONCLUSION

PET images of AD subjects show different laminar distributions of tau and Aβ deposits. Tau pathology tends to localize in the deeper lamina of the cortical ribbon, whereas the Aβ is more uniformly distributed. This observation may lead to a new biomarker of AD progression. It may also be of use in the evaluation of other neurodegenerative disorders with different tau distributions.

DISCLOSURE

The costs of publication of this article were defrayed in part by the payment of page charges. Therefore, and solely to indicate this fact, this article is hereby marked "advertisement" in accordance with 18 USC section 1734. Work at NYU was supported by

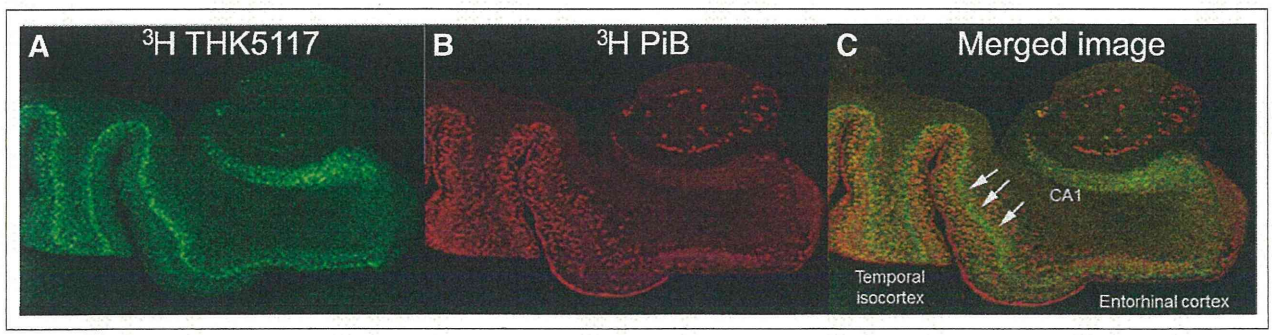

FIGURE 4. AD autoradiography images: ^{3}H-THK5117 (green) (A), ^{3}H-PiB (red) (B), and overlapping tau and amyloid binding (orange) (C). Arrows highlight more inferior tau pathology distribution.

NIH/NIA grants AG035137, AG032554, AG022374, AG013616, and AG012101 and by the Steven and Alexandra Cohen Veterans Center. Work at Tohoku University was supported by Health and Labor Sciences research grants from the Ministry of Health, Labor, and Welfare of Japan, a Grant-in-Aid for Scientific Research (B) (23390297), a Grant-in-Aid for Scientific Research on Innovative Areas (26117003), a grant from the Japan Advanced Molecular Imaging Program (J-AMP) of the Ministry of Education, Culture, Sports, Science and Technology, and the research fund from GE Healthcare and Sumitomo Electric Industries, Ltd. No other potential conflict of interest relevant to this article was reported.

ACKNOWLEDGMENT

Yi Li is a PhD student at Shandong University. This work partially fulfills Yi Li's PhD degree requirements. Both Shandong University and New York University are primary affiliations of Yi Li.

REFERENCES

1. Hyman BT, Trojanowski JQ. Consensus recommendations for the postmortem diagnosis of Alzheimer disease from the National Institute on Aging and the Reagan Institute working group on diagnostic criteria for the neuropathological assessment of Alzheimer disease. *J Neuropathol Exp Neurol.* 1997;56:1095–1097.
2. Thal DR, Rub U, Orantes M, Braak H. Phases of A beta-deposition in the human brain and its relevance for the development of AD. *Neurology.* 2002;58:1791–1800.
3. Braak H, Braak E. Neuropathological stageing of Alzheimer-related changes. *Acta Neuropathol.* 1991;82:239–259.
4. Hof PR, Bouras C, Buee L, Delacourte A, Perl DP, Morrison JH. Differential distribution of neurofibrillary tangles in the cerebral cortex of dementia pugilistica and Alzheimer's disease cases. *Acta Neuropathol.* 1992;85:23–30.
5. Klunk WE, Engler H, Nordberg A, et al. Imaging brain amyloid in Alzheimer's disease with Pittsburgh compound-B. *Ann Neurol.* 2004;55:306–319.
6. Chien DT, Szardenings AK, Bahri S, et al. Early clinical PET imaging results with the novel PHF-tau radioligand [F18]-T808. *J Alzheimers Dis.* 2014;38:171–184.
7. Okamura N, Furumoto S, Fodero-Tavoletti MT, et al. Non-invasive assessment of Alzheimer's disease neurofibrillary pathology using ^{18}F-THK5105 PET. *Brain.* 2014;137:1762–1771.
8. Ishiki A, Furumoto S, Harada R, et al. Accumulation of the novel tau imaging tracer ^{18}F-THK-5117 is associated with brain atrophy in Alzheimer's disease [abstract]. *Alzheimers Dement.* 2014;10(suppl):P131.
9. Okamura N, Furumoto S, Harada R, et al. Novel ^{18}F-labeled arylquinoline derivatives for noninvasive imaging of tau pathology in Alzheimer disease. *J Nucl Med.* 2013;54:1420–1427.
10. Rowe CC, Ng S, Ackermann U, et al. Imaging beta-amyloid burden in aging and dementia. *Neurology.* 2007;68:1718–1725.
11. Rahmim A, Qi J, Sossi V. Resolution modeling in PET imaging: theory, practice, benefits, and pitfalls. *Med Phys.* 2013;40:064301.
12. Mungas D, Tractenberg R, Schneider JA, Crane PK, Bennett DA. A 2-process model for neuropathology of Alzheimer's disease. *Neurobiol Aging.* 2014;35:301–308.
13. Baugh CM, Stamm JM, Riley DO, et al. Chronic traumatic encephalopathy: neurodegeneration following repetitive concussive and subconcussive brain trauma. *Brain Imaging Behav.* 2012;6:244–254.

Eur J Nucl Med Mol Imaging (2014) 41:816–826
DOI 10.1007/s00259-013-2681-7

ORIGINAL ARTICLE

In vivo evaluation of a novel tau imaging tracer for Alzheimer's disease

Victor L. Villemagne · Shozo Furumoto · Michelle T. Fodero-Tavoletti · Rachel S. Mulligan · John Hodges · Ryuichi Harada · Paul Yates · Olivier Piguet · Svetlana Pejoska · Vincent Doré · Kazuhiko Yanai · Colin L. Masters · Yukitsuka Kudo · Christopher C. Rowe · Nobuyuki Okamura

Received: 14 October 2013 / Accepted: 20 December 2013 / Published online: 11 February 2014

Abstract
Purpose Diagnosis of tauopathies such as Alzheimer's disease (AD) still relies on post-mortem examination of the human brain. A non-invasive method of determining brain tau burden in vivo would allow a better understanding of the pathophysiology of tauopathies. The purpose of the study was to evaluate ^{18}F-THK523 as a potential tau imaging tracer.

Methods Ten healthy elderly controls, three semantic dementia (SD) and ten AD patients underwent neuropsychological examination, MRI as well as ^{18}F-THK523 and ^{11}C-Pittsburgh compound B (PIB) positron emission tomography (PET) scans. Composite memory and non-memory scores, global and hippocampal brain volume, and partial volume-corrected tissue ratios for ^{18}F-THK523 and ^{11}C-PIB were estimated for all participants. Correlational analyses were performed between global and regional ^{18}F-THK523, ^{11}C-PIB, cognition and brain volumetrics.

Results ^{18}F-THK523 presented with fast reversible kinetics. Significantly higher ^{18}F-THK523 retention was observed in the temporal, parietal, orbitofrontal and hippocampi of AD patients when compared to healthy controls and SD patients. White matter retention was significantly higher than grey matter retention in all participants. The pattern of cortical ^{18}F-THK523 retention did not correlate with Aβ distribution as assessed by ^{11}C-PIB and followed the known distribution of tau in the AD brain, being higher in temporal and parietal areas than in the frontal region. Unlike ^{11}C-PIB, hippocampal ^{18}F-THK523 retention was correlated with several cognitive parameters and with hippocampal atrophy.

Conclusion ^{18}F-THK523 does not bind to Aβ in vivo, while following the known distribution of paired helical filaments (PHF)-tau in the brain. Significantly higher cortical ^{18}F-THK523 retention in AD patients as well as the association of hippocampal ^{18}F-THK523 retention with cognitive parameters and hippocampal volume suggests ^{18}F-THK523 selectively binds to tau in AD patients. Unfortunately, the very high ^{18}F-THK523 retention in white matter precludes simple visual inspection of the images, preventing its use in research or clinical settings.

Keywords Alzheimer's disease · Tau imaging · Aβ Imaging · Neurodegeneration · Brain

Electronic supplementary material The online version of this article (doi:10.1007/s00259-013-2681-7) contains supplementary material, which is available to authorized users.

V. L. Villemagne · M. T. Fodero-Tavoletti · R. S. Mulligan · P. Yates · S. Pejoska · V. Doré · C. C. Rowe
Centre for PET, Austin Health, Melbourne, Australia

V. L. Villemagne · M. T. Fodero-Tavoletti · C. L. Masters
The Mental Health Research Institute, Melbourne, Australia

S. Furumoto · R. Harada · K. Yanai · N. Okamura
Department of Pharmacology, Tohoku University School of Medicine, Sendai, Japan

J. Hodges · O. Piguet
Neuroscience Research Australia, Sydney, Australia

J. Hodges · O. Piguet
The University of New South Wales, Sydney, Australia

V. Doré
Preventative Health Flagship, CSIRO ICT, Brisbane, Australia

Y. Kudo
Innovation of New Biomedical Engineering Center, Tohoku University, Sendai, Japan

V. L. Villemagne (✉)
Department of Nuclear Medicine and Centre for PET, Austin Health, 145 Studley Rd, Heidelberg, VIC 3084, Australia
e-mail: villemagne@petnm.unimelb.edu.au